

Cryo-EM reveals the steric zipper structure of a light chain-derived amyloid fibril

Andreas Schmidt^a, Karthikeyan Annamalai^a, Matthias Schmidt^a, Nikolaus Grigorieff^{b,1}, and Marcus Fändrich^{a,1}

^aInstitute of Protein Biochemistry, Ulm University, 89081 Ulm, Germany; and ^bJanelia Research Campus, Howard Hughes Medical Institute, Ashburn, VA 20147

Edited by Robert M. Glaeser, Lawrence Berkeley National Laboratory, Berkeley, CA, and accepted by the Editorial Board April 11, 2016 (received for review November 11, 2015)

Amyloid fibrils are proteinaceous aggregates associated with diseases in humans and animals. The fibrils are defined by intermolecular interactions between the fibril-forming polypeptide chains, but it has so far remained difficult to reveal the assembly of the peptide subunits in a full-scale fibril. Using electron cryomicroscopy (cryo-EM), we present a reconstruction of a fibril formed from the pathogenic core of an amyloidogenic immunoglobulin (Ig) light chain. The fibril density shows a lattice-like assembly of face-to-face packed peptide dimers that corresponds to the structure of steric zippers in peptide crystals. Interpretation of the density map with a molecular model enabled us to identify the intermolecular interactions between the peptides and rationalize the hierarchical structure of the fibril based on simple chemical principles.

FreeRx | prion | protein aggregation | protein folding | systemic amyloidosis

Amyloid fibrils are best known for their association with diseases, including Alzheimer's, Parkinson's, and the various forms of systemic amyloidosis (1). However, amyloid fibrils can also be functional in vivo (1), and there is increasing interest in the potential of the filaments as the basis of new biomaterials and nanotechnological devices (2). The common structural motif of all these fibrils is an intermolecular stack of β -strands, termed the fibril cross- β conformation (3). Previous analyses with NMR, electron cryomicroscopy (cryo-EM), and other techniques have provided information on the assembly of the polypeptide chains in the fibril and illuminated the residue-specific conformation (4–6) and overall properties of these fibrils, such as their handedness, polarity, and symmetry (7–13). By contrast, it has remained difficult to determine the orientation and assembly of the polypeptide chains relative to one another and the intermolecular interactions between the molecules within a full-scale fibril.

Valuable insights into the interactions in cross- β -sheets have previously come from the study of steric zippers in peptide microcrystals. Steric zippers represent pairs of self-complementary β -sheets that are formed by very short peptides (14, 15). Although zippers were suggested to constitute the structural spines of amyloid fibrils formed from usually much longer polypeptide chains (16, 17), their role for fibril formation remains controversial. For example, solid-state NMR data suggest that the peptide conformations in fibrils and microcrystals differ even when formed from the same peptide (18). Ultrasound measurements revealed the presence of packing defects and of cavities within fibril structures (19), whereas steric zippers typically show a very dense packing (14, 15). Previously described fibril and steric zipper structures also differed in their β -sheet architecture. Microcrystals usually comprised untwisted β -sheets (14, 15), whereas β -sheets were characteristically twisted in fibrils (7–11, 20–22). Finally, even in those cases where a zipper was implicated in the structure of a fibril, it included only a relatively small portion of the fibril cross- β structure (16, 17). Hence, steric zippers explained only a minor fraction of the interactions stabilizing these fibrils.

In this study, we took advantage of recently improved cryo-EM methodologies (23) and identified the peptide assembly of a fibril

formed from a peptide fragment of a human pathogenic AL protein. AL proteins are full-length or fragmented Ig light chains (LCs) that constitute the fibrils giving rise to AL amyloidosis (24). The heart is a frequent site of fibril deposition, and pathology depends, at least partly, on severe distortions and a compromised functionality of the organ affected by large fibril deposits. We find that the analyzed fibril consists of a lattice-like assembly of peptide dimers that reproduces the structure of steric zippers in peptide microcrystals. Therefore, our data support the hypothesis that steric zipper structures can underlie the formation of a full-scale fibril.

Results

Identification of the Amyloid Core Structure of Pathogenic LCs. A fibril-forming λ -LC protein (25) was analyzed with five different algorithms to identify its amyloidogenic core (Fig. 1*A*). Synthetic peptides from two segments were obtained that were predicted to be particularly amyloidogenic and further corresponded to β -strand conformation in the globular LC protein (Fig. 1*A* and *B*). We termed these segments AL1 and AL2. The two segments comprise aromatic residues to aid in experimental detection and cover different degrees of sequential conservation. AL1 corresponds to the complementarity-determining regions (CDRs), which reflect the variability of AL proteins, whereas AL2 originates from a conserved segment of the constant domain. We experimentally confirmed their high propensity to form fibrils as incubation led to large quantities of fibrils as shown by EM (Fig. 1*C* and *D*).

Significance

Previous studies suggested that the interactions within amyloid fibrils correspond to those seen in peptide microcrystals consisting of steric zippers. Using electron cryomicroscopy, we can now provide further evidence for this hypothesis in a fibril structure that consists of peptide dimers forming steric zippers. These zippers are arranged in a periodic fibrillar lattice, similar to the periodic structure of a crystal. The fibril structure can be rationalized as a hierarchical assembly that is based on simple chemical principles. Identifying the chemical principles that drive fibril formation may deepen our understanding of human diseases linked to these fibrils and of functional amyloids underlying vital biological functions. Furthermore, it may enable novel biotechnological applications and the design of new fibril-based nanomaterials.

Author contributions: N.G., and M.F. designed research; A.S., K.A., and M.S. performed research; A.S., K.A., M.S., N.G., and M.F. analyzed data; and A.S., K.A., N.G., and M.F. wrote the paper.

The authors declare no conflict of interest.

This article is a PNAS Direct Submission. R.M.G. is a guest editor invited by the Editorial Board.

Data deposition: The structure of the fibril has been deposited in the Electron Microscopy Data Bank (accession no. EMD-3128).

¹To whom correspondence may be addressed. Email: marcus.faendrich@uni-ulm.de or niko@grigorieff.org.

This article contains supporting information online at www.pnas.org/lookup/suppl/doi:10.1073/pnas.1522282113/-DCSupplemental.

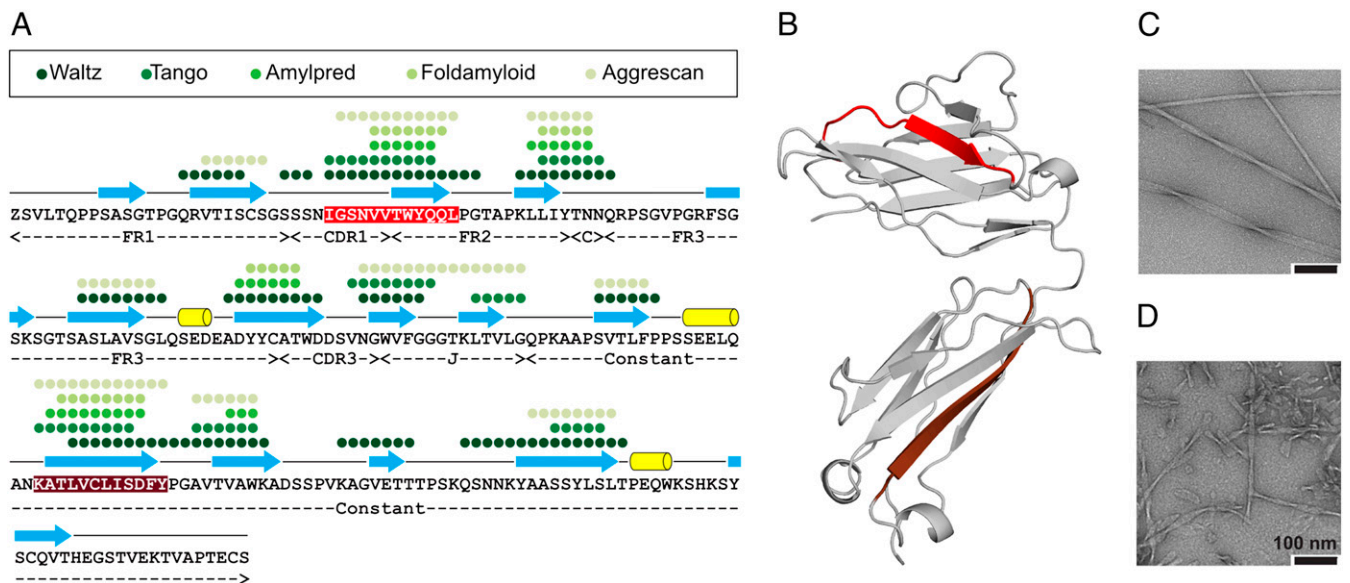


Fig. 1. Identification of the amyloid core of a human pathogenic AL protein. (A) Residue-specific prediction of amyloid core within an AL protein (25) by five different algorithms as indicated in the panel. Red, AL1; brown, AL2. The assignment of secondary structural elements is based on the homologous λ -LC from B. Blue, β -strand; yellow, α -helix. (B) Ribbon diagram of a homologous λ -LC crystal structure (Protein Data Bank entry 4BJL) (26). A and B use the same color coding. (C and D) Negative stain TEM images of fibrils from peptides AL1 (C) and AL2 (D).

Both peptides adopted multiple fibril morphologies, but AL1 peptide fibrils were particularly long and straight, and associated with a more regular crossover structure. These features made AL1 peptide fibrils suitable for cryo-EM and 3D reconstruction, and all further experiments were performed with this peptide sample. The AL1 peptide segment also encompasses one of the major sites determining the amyloidogenicity of λ AL proteins, as revealed by a comparison of the amyloid score of AL protein variable LC (V_L) domains from $\lambda 1$, $\lambda 2$, $\lambda 3$, and $\lambda 6$ LCs, the major λ -subtypes causing AL amyloidosis (Fig. S1).

Cryo-EM Reveals Fibrils with a Lattice Consisting of Rhombic Building Blocks. AL1 peptide fibrils exhibited classical amyloid characteristics, such as Congo red (CR) green birefringence and X-ray diffraction (XRD) reflections at about 4.7 Å and 10 Å (Fig. S2). Unidirectional platinum shadowing demonstrated their left-handed helical architecture (Fig. S3). Using cryo-EM, we identified one fibril morphology suitable for further image processing (Fig. 2A). We obtained a reconstruction at a spatial resolution of 9.8 Å (Table S1) that was compatible with a twofold helical symmetry and a polar fibril topology (Fig. 2B and C). Projections of the reconstruction match the raw cryo-EM images obtained from

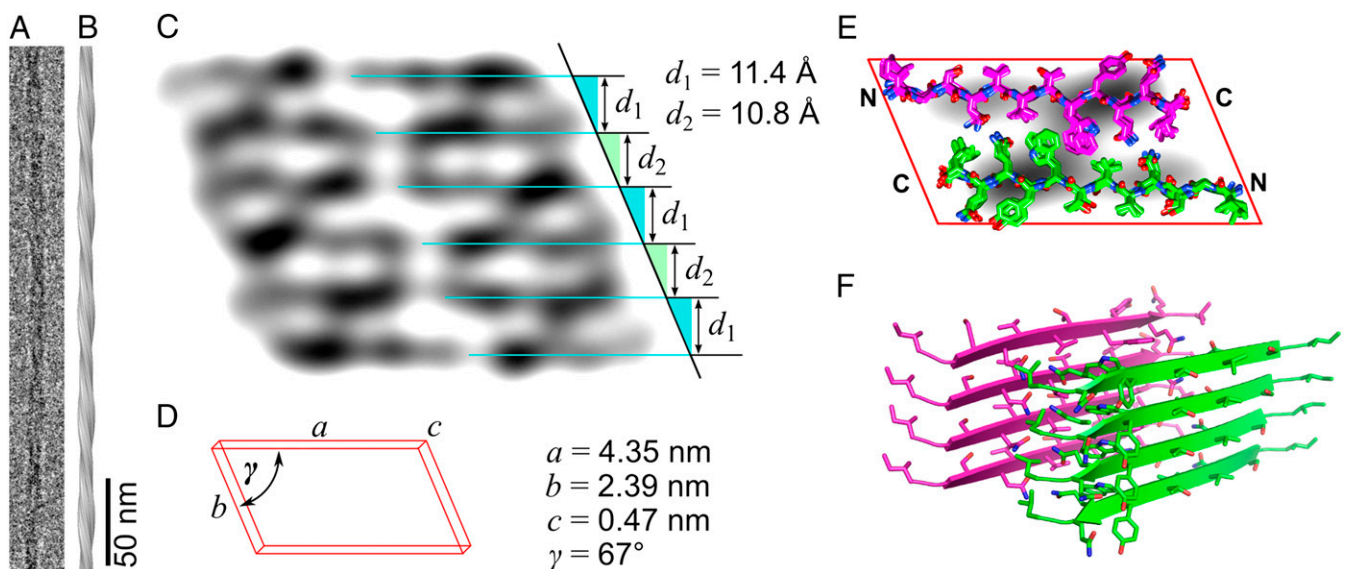


Fig. 2. Cryo-EM images and structural reconstructions. (A) Cryo-EM image, (B) side view, and (C) cross-section of the reconstructed fibril. Spacings d_1 and d_2 refer to the packing distances within the dimer and between adjacent dimers, respectively. (D) Schematic representation of the basic building block of the fibril. The fibril cross-section (C) contains six of these building blocks. (E) Cross-sectional view of a family of six structural models of the peptide dimer superimposed with the averaged density of the six building blocks of the fibril. (F) Side view of a stack of four hydrogen-bonded peptide dimers. The side chain conformations shown in the model are not determined by the density and only represent possible conformations that are compatible with the packing shown here.

these fibrils (see *Analysis of the Peptide Assembly in the Fibril*). Through a cross-correlation analysis (see *SI Materials and Methods*), we found the fibril to be constructed from equally spaced building blocks ($a = 4.35$ nm, $b = 2.39$ nm, and $\gamma = 67^\circ$) that, taken together with a cross- β spacing of $c = 4.69 \pm 0.05$ Å observed by XRD (Fig. S2), outline a rhombic building block as the basic structural element of the analyzed fibrils (Fig. 2 D and E).

Each Building Block Contains a Face-to-Face Packed Peptide Dimer.

Each building block comprises two elongated density regions that correspond to the size of two 12-residue peptide molecules in β -strand conformation suggesting a total of six peptide dimers per cross- β repeat for this fibril morphology (Fig. 2 C and E). The distribution of large-sized and small-sized amino acid residues in the AL1 peptide (sequence IGSNVVTWYQQL) matches the observed density distribution of the two elongated regions and defines the N-to-C orientation of the peptides in cross-section. The two density regions are related by quasi-twofold symmetry, indicating a face-to-face packing of the peptide dimer (Fig. 2E). The peptides are 11.4 ± 0.7 Å apart in the dimer and 10.8 ± 0.8 Å apart between neighboring dimers (Fig. 2C). These values roughly correlate with the XRD pattern of AL1 peptide fibrils showing a broad

side chain reflection at 10–11 Å (Fig. S2). The resulting assembly of the two peptides is such that the backbone hydrogen bond donor and acceptor groups point in the direction of the fibril axis, and the side chains face the adjacent peptides (Fig. 2F). Stacking multiple dimers in the direction of the main fibril axis results in a protofilament that consists of a pair of two self-complementary, parallel cross- β -sheets (Fig. 2F). The fibril contains six protofilaments (Fig. 3 A and B), which is consistent with scanning transmission electron microscopy (TEM) and mass-per-length measurements, yielding a histogram with a peak close to 12 peptide molecules per cross- β repeat (Fig. S4).

Analysis of the Peptide Assembly in the Fibril. To analyze the assembly of the peptides in the fibril in more detail, we generated a series of atomic models that sampled systematically altered arrangements of two peptides within the dimer but retained the overall peptide orientation as described in *Each Building Block Contains a Face-to-Face Packed Peptide Dimer*. We specifically tested alternative peptide registers and staggered and nonstaggered β -sheet assemblies, as well as peptide orientations that were flipped by 180° (Fig. S5). We then evaluated the consistency of these models with the observed β -sheet packing distance (Table S2), the XRD pattern

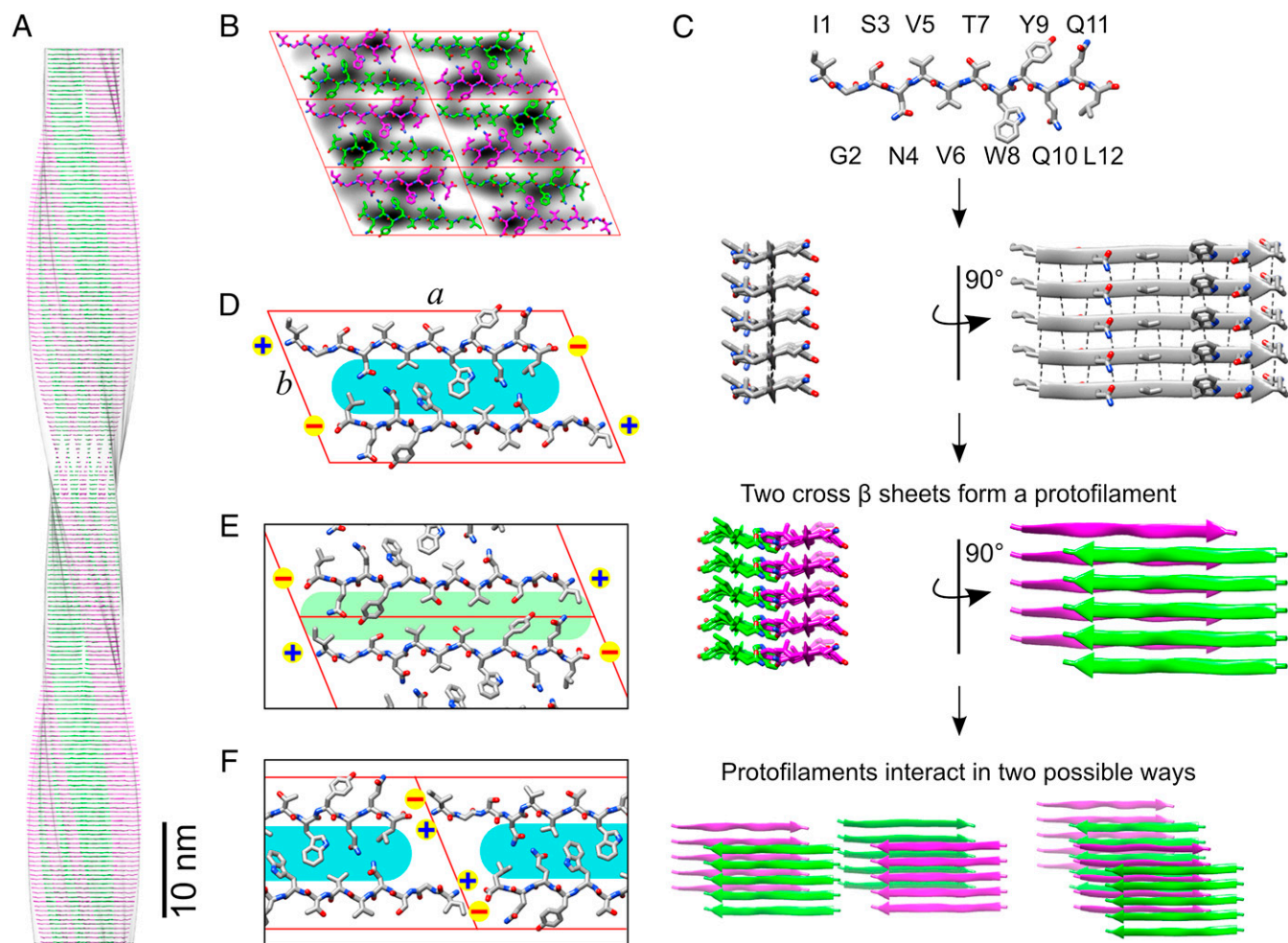


Fig. 3. Peptide packing into a hierarchically structured fibril. (A) Side view of a stack of 200 peptide layers (green, magenta) and (B) cross-section superimposed with the density (gray). (C) Structural hierarchy of the fibril. Extended rod-like AL1 peptide molecules pack into a cross- β -sheet via backbone hydrogen bonds and interactions between nonionic side chains. Two cross- β -sheets form a face-to-face packed dimer (protofilament). Six of these protofilaments packed together form the fibril described in this study. (D) Packing of the peptides within the protofilament cross-section. (E) Side-by-side packing of two protofilaments along axis b . (F) Head-to-tail packing of two protofilaments along axis a . The side chain conformations shown in the model are not determined by the density and only represent possible conformations that are compatible with the packing shown here.

(Fig. S5), and basic chemical principles, such as the burial of hydrophobic amino acid residues (Table S2).

We found that the best fit of our data was obtained with an arrangement that places the even-numbered residues (Asn4, Val6, Trp8, Gln10, Leu12) at the peptide intradimer interface while the odd-numbered residues (Ile1, Ser3, Val5, Thr7, Tyr9, Gln11) are at the interdimer interface (Table S2, dimer A). Using the average van der Waals (v.d.W.) volumes of the residues at the interaction surface (120.4 \AA^3 within the dimer and 108.3 \AA^3 between the dimers) and a previously described empirical correlation between v.d.W. volume and cross- β -sheet packing distance (27), we predicted packing distances of 11.6 \AA and 10.1 \AA within and between the dimers, respectively. These values agree well with the distances between the density maxima in our map (Fig. 2C). There was also good agreement between projections of the models, the corresponding raw data, and the projections of the reconstructed AL1 peptide fibrils (Fig. S6). In addition, we noted that the average hydrophobicity of the amino acids forming the intradimer interface (-1.26 kcal/mol), as well as the interdimer interface if packed along axis b (-0.92 kcal/mol), is greatest in this model (Table S2).

None of the alternatively tested models was able to satisfy all of the identified constraints: They did not fit well with the packing distances indicated by the density maxima within the building block (Fig. 2C and Table S2), altered the complementarity of polar and hydrophobic residues of adjacent peptides (Fig. S5, dimers B and C), and/or produced a split of the meridional reflection of the power spectrum that was not seen in the XRD pattern (Fig. S5). Therefore, we conclude that the model featuring an unstaggered cross- β -sheet and a peptide dimer with an interface of odd-numbered residues provides the best explanation for our structural data (Fig. 3A and B).

Assembly Principles of the AL1 Peptide Fibril. Using that model, it is possible to explain the structural hierarchy of the fibril based on simple chemical principles (Fig. 3C). In the following, we divide this structural hierarchy into four levels.

- i) At the first level is the conformation of the peptide in the fibril (Fig. 3C). AL1 peptide adopts a largely extended conformation in the fibril and a β -strand conformation in the LC precursor protein (Fig. 1B). This finding is consistent with its sequence, which indicates a uniformly high propensity to form a cross- β structure (Fig. 1A).
- ii) At the second hierarchical level is the formation of a cross- β -sheet. The rod-like conformation of the peptide enables its packing into relatively flat cross- β -sheets. A single sheet is stabilized by intermolecular interactions that run in the direction of the fibril axis, that is, by β -sheet hydrogen bonds of the peptide backbone as well as contacts between the side chains of the hydrogen-bonded molecules (Fig. 3C). These side chain–side chain interactions are inevitably hydrophobic or polar in nature, as AL1 peptide lacks fully ionizable amino acid residues. In addition, there may be π stacking interactions between the side chains of Trp8.
- iii) At the third level of the structural hierarchy is the arrangement of the multiple cross- β -sheets into a protofilament. The AL1 peptide fibril protofilament consists of two cross- β -sheets that interact by their even-numbered amino acid residues (Fig. 3D). An interaction through the even-numbered rather than the odd-numbered residues causes Trp8 to be buried within the protofilament core. Furthermore, this leads to an average hydrophobicity of the amino acid residues forming the interaction surface that is notably higher than in models where the two sheets of the protofilaments interact by the odd-numbered residues (Table S2). There is also a good steric and chemical fit of the two peptides, as there are intermolecular interactions between Trp8 and Val6, and between Asn4 and Gln10 (Fig. 3D).
- iv) At the fourth level of structural hierarchy is the assembly of multiple protofilaments into a mature fibril. According to our

data, AL1 peptide protofilaments can interact only in two possible modes. The first mode involves side-by-side packing of the peptide dimers within the fibril cross-section along axis b (Fig. 3E) such that the dimers interact via their hydrophobic or polar amino acid side chains. The second mode of interaction corresponds to head-to-tail packing of the peptide dimers in the cross-section along axis a (Fig. 3F) such that the contact area between two protofilaments is formed by the complementary charges of the peptide N and C termini.

Discussion

High-resolution structural information on amyloid-like fibrils remains scarce due to the difficulty of obtaining homogeneous preparations of fibrils and a sufficient number of intramolecular and intermolecular structural constraints that could enable structure determination by solid-state NMR, and because fibrils have not been crystallized for crystallographic studies. The discovery of steric zippers in microcrystals of small peptide fragments provided a glimpse of what type of interactions may be responsible for stabilizing amyloid fibrils and how the characteristic $\sim 10\text{-\AA}$ XRD maximum arises (14, 15). However, until recently, steric zippers were not directly observed in fibrils, which typically form from significantly longer peptides and exhibit a helical twist that is not present in the microcrystals. It has therefore remained unclear how closely crystal and fibril structures are related and, therefore, how much can be learned about the fundamental principles of fibril formation and properties from crystal structures.

Our cryo-EM reconstruction of a peptide fibril derived from a human pathogenic AL protein provides a clear link between fibrils and crystals by exhibiting structural elements typical for both. The AL1 peptide fibril protofilament consists of two self-complementary cross- β -sheets and thus shows an arrangement that effectively corresponds to that of a steric zipper. The presence of steric zippers and the lattice-like arrangement of protofilaments mimics the structure of a crystal, and the helical twist and elongated appearance are typical for amyloid fibrils. The structure of this fibril can be explained based on simple hydrophobic and ionic interactions that result in the lattice-like arrangement of face-to-face packed dimers (Fig. 3B). Face-to-face packed dimers are also present in other types of amyloid-like fibrils formed by Alzheimer's A β (1-40) and A β (1-42) peptide and may point to an assembly pathway that starts with the formation of dimers (7, 9). Although steric zippers are likely also present in A β fibrils (17), they describe only the interaction between small segments of the A β peptide, making a full description of principles of fibril formation more difficult. In the case of the AL1 peptide fibril we imaged here, the steric zipper extends along most of the peptide dimer interface, making it the predominant structural feature. With 12 amino acids in the peptide, this zipper is the longest observed to date.

Our data further establish the peptide dimer motif as one of the major themes of structuring amyloids (Fig. S7). This motif was previously seen by X-ray crystallography in microcrystals encompassing steric zipper structures, and by cryo-EM in the fibrils formed from AL1, A β (1-40), and A β (1-42) peptides (7, 9). Furthermore, there is solid-state NMR evidence for peptide dimers in fibrils formed from a transthyretin-derived peptide fragment (11), an N-terminally extended variant of A β (1-40) (28), and from an A β peptide variant carrying the Osaka mutation (29). The peptide dimer motif was also found in several structural models of longer polypeptide chains, such as ribonuclease A (16, 17, 30). Most of these studies report the dimer interface to be arranged face to face, similar to the arrangement found in the present study (Fig. 2E), and, indeed, a face-to-face assembly can explain the dimeric fibril substructure better than a face-to-back arrangement, which would not necessarily be confined to dimers and could be readily extended into trimers, tetramers, etc. The peptide dimer is one of several possible structural themes in the assembly of amyloids that

also include β -arch-derived conformations, such as β -solenoid helices or β -meander structures (Fig. S7).

Although peptide conformation and packing may differ from those observed here, the AL1 peptide segment is likely also at the cross- β core of tissue-deposited AL amyloid fibrils because sequence comparisons imply that it represents one of the major amyloidogenic sites with AL protein V_L domains from $\lambda 1$, $\lambda 2$, $\lambda 3$, and $\lambda 6$ LCs (Fig. S1). The AL1 peptide segment lacks fully ionizable side chains. Hence, the way of packing into protofilaments may be different for AL proteins containing ionizable side chains in the AL1 peptide region compared to the one described here (Fig. 3C). The AL1 peptide segment corresponds mainly to strand C of the native β -sandwich structure (Fig. 1A) and, together with strand C', forms a β -hairpin that can potentially flip out of the folded protein domain to form amyloid under oxidative conditions. Analysis of the structure of acid-unfolded V_L domains by NMR spectroscopy further revealed the AL1 peptide segment to be largely unfolded in the V_L domain of wild-type AL protein under oxidative conditions and to be significantly structured within two control V_L domains that originated from LCs not associated with AL amyloidosis (31). It is also interesting to note that the V_L Ig domain is topologically related to the β -sandwich structure of $\beta 2$ -microglobulin, another protein that can give rise to amyloid inside the body and that was analyzed with cryo-EM (13). However, the pattern of amyloidogenic sites is different in $\beta 2$ -microglobulin and may not substantially depend on the strand, which is topologically homologous to strand C within V_L domains (15) studied here.

Knowledge of the peptide-peptide interactions in amyloid fibrils is not only important for understanding their role and formation in the course of debilitating human diseases. Peptide fibrils with amyloid properties may also have functional properties *in vivo* (1) or be relevant for a broad range of possible biotechnological applications, such as viral transfection enhancers, templated metal wires, and peptide scaffolds for cell growth (32–35). In our present analysis of the AL1 peptide fibrils, we are able to rationalize the observed structure in terms of a few basic chemical interactions that may permit the assembly of other fibril structures from designed peptides. Understanding the principles of cross- β assemblies and the formation of protein fibril assemblies is thus of considerable importance for understanding the biological and material properties of amyloid structures beyond understanding the molecular basis of disease.

Materials and Methods

Transmission Cryo-EM. Three microliters of the fibril solution (14 $\mu\text{g}/\text{mL}$) were placed onto glow-discharged C-flat (Protochips) holey carbon grid (CF 1.2/1.3-2C),

backside blotted, and plunged into liquid ethane. Samples were examined under an FEI Tecnai F20 electron microscope operating at 200 kV and using a magnification of 66,000 \times . The electron dose used for imaging was $\sim 20 \text{ e}/\text{\AA}^2$.

Image Processing. For image acquisition, we used an FEI Falcon 1 direct electron detector with an effective pixel size of 2.11 \AA at the specimen level. Images were selected for micrograph and fibril quality. Crossover distances of AL1 peptide fibrils were limited to $56.9 \pm 3.8 \text{ nm}$. Eleven fibrils were selected using EMAN's boxer program (36). Single-particle reconstruction of the fibril with the SPIDER software package (37) at a pixel size of 8.44 \AA was initially carried out without imposing symmetry and revealed twofold symmetry. For later reconstructions with the FREALIX software (23), twofold symmetry was imposed, and reconstructions of $60.35 \times 60.35 \times 60.35 \text{ nm}$ in size were obtained. FREALIX also determined the polarity of the analyzed fibrils to ensure their correct alignment during the reconstruction. Fibrils with a crossover distance of less than 53.1 nm and larger than 60.7 nm were excluded. FREALIX segments a fibril along its path and assigns coordinates and angles to each segment that define its alignment within the twisted fibril. By using these angles and coordinates for the reconstruction, FREALIX takes into account deviations from a perfect helical symmetry. These angles and coordinates were refined using restraints derived by modeling full filaments (full-filament mode), which enforces a continuous filament geometry. Helical symmetry was imposed using a rotation of 1.46° per repeat. The resolution of the reconstructed fibril was estimated using the 0.5 and 0.143 thresholds of the Fourier shell correlation curve (Table S1).

Peptide Modeling. The reconstructed density of fibril morphology I was sharpened using the program *bfactor.exe* (38) using a B-factor of -500 \AA^2 , and was low-pass filtered at 10 \AA resolution. A 6.33- \AA slice was cut out from the corrected map. Three pairs of building blocks along axis *b* were masked, aligned to each other, and averaged using the program SPIDER. Models of the peptide assuming a uniform distribution of Φ/Ψ dihedral angles of $-139^\circ/135^\circ$, compatible with β -strand conformation, were modeled and superimposed with the cross-sectional slice using COOT (39) and Chimera (40) to fit the density.

Fibril formation and Characteristics. Prediction of the amyloid-prone regions, the conditions of fibril formation, XRD, CR green birefringence, the calculation of the power spectra as well as negative stain, and scanning TEM methods are described in *SI Materials and Methods*.

Graphical Representation of Protein Structures. These methods are described in *SI Materials and Methods*.

ACKNOWLEDGMENTS. We thank Paul Walther for assistance in platinum shadowing, Alexis Rohou for help with the use of the FREALIX software, Joe Wall for assistance with mass-per-length measurements, and Ute Hegenbart and Stefan Schönland for helpful discussions. This work is supported by grants from German Federal Ministry of Education and Research (GERAMY-network, 01GM1107D) and the National Institutes of Health (P01 GM62580, awarded to N.G.).

- Chiti F, Dobson CM (2006) Protein misfolding, functional amyloid, and human disease. *Annu Rev Biochem* 75:333–366.
- Knowles TP, Buehler MJ (2011) Nanomechanics of functional and pathological amyloid materials. *Nat Nanotechnol* 6(8):469–479.
- Sunde M, et al. (1997) Common core structure of amyloid fibrils by synchrotron X-ray diffraction. *J Mol Biol* 273(3):729–739.
- Su Y, Andreas L, Griffin RG (2015) Magic angle spinning NMR of proteins: High-frequency dynamic nuclear polarization and (1)H detection. *Annu Rev Biochem* 84:465–497.
- Wasmer C, et al. (2008) Amyloid fibrils of the HET-s(218-289) prion form a beta solenoid with a triangular hydrophobic core. *Science* 319(5869):1523–1526.
- Lührs T, et al. (2005) 3D structure of Alzheimer's amyloid-beta(1-42) fibrils. *Proc Natl Acad Sci USA* 102(48):17342–17347.
- Sachse C, Fändrich M, Grigorieff N (2008) Paired beta-sheet structure of an Abeta(1-40) amyloid fibril revealed by electron microscopy. *Proc Natl Acad Sci USA* 105(21):7462–7466.
- Meinhardt J, Sachse C, Hortschansky P, Grigorieff N, Fändrich M (2009) Abeta(1-40) fibril polymorphism implies diverse interaction patterns in amyloid fibrils. *J Mol Biol* 386(3):869–877.
- Schmidt M, et al. (2015) Peptide dimer structure in an A β (1-42) fibril visualized with cryo-EM. *Proc Natl Acad Sci USA* 112(38):11858–11863.
- Zhang R, et al. (2009) Interprotofilament interactions between Alzheimer's Abeta1-42 peptides in amyloid fibrils revealed by cryoEM. *Proc Natl Acad Sci USA* 106(12):4653–4658.
- Fitzpatrick AW, et al. (2013) Atomic structure and hierarchical assembly of a cross- β amyloid fibril. *Proc Natl Acad Sci USA* 110(14):5468–5473.
- Mizuno N, Baxa U, Steven AC (2011) Structural dependence of HET-s amyloid fibril infectivity assessed by cryoelectron microscopy. *Proc Natl Acad Sci USA* 108(8):3252–3257.
- White HE, et al. (2009) Globular tetramers of beta(2)-microglobulin assemble into elaborate amyloid fibrils. *J Mol Biol* 389(1):48–57.
- Nelson R, et al. (2005) Structure of the cross-beta spine of amyloid-like fibrils. *Nature* 435(7043):773–778.
- Sawaya MR, et al. (2007) Atomic structures of amyloid cross-beta spines reveal varied steric zippers. *Nature* 447(7143):453–457.
- Wiltzius JJ, et al. (2009) Molecular mechanisms for protein-encoded inheritance. *Nat Struct Mol Biol* 16(9):973–978.
- Colletier JP, et al. (2011) Molecular basis for amyloid-beta polymorphism. *Proc Natl Acad Sci USA* 108(41):16938–16943.
- van der Wel PC, Lewandowski JR, Griffin RG (2007) Solid-state NMR study of amyloid nanocrystals and fibrils formed by the peptide GNNQQNY from yeast prion protein Sup35p. *J Am Chem Soc* 129(16):5117–5130.
- Lee YH, Chatani E, Sasahara K, Naiki H, Goto Y (2009) A comprehensive model for packing and hydration for amyloid fibrils of beta2-microglobulin. *J Biol Chem* 284(4):2169–2175.
- Jiménez JL, et al. (1999) Cryo-electron microscopy structure of an 5H3 amyloid fibril and model of the molecular packing. *EMBO J* 18(4):815–821.
- Jiménez JL, et al. (2002) The protofilament structure of insulin amyloid fibrils. *Proc Natl Acad Sci USA* 99(14):9196–9201.
- Blake C, Serpell L (1996) Synchrotron X-ray studies suggest that the core of the transthyretin amyloid fibril is a continuous beta-sheet helix. *Structure* 4(8):989–998.
- Rohou A, Grigorieff N (2014) FREALIX: Model-based refinement of helical filament structures from electron micrographs. *J Struct Biol* 186(2):234–244.
- Blancas-Mejía LM, Ramirez-Alvarado M (2013) Systemic amyloidoses. *Annu Rev Biochem* 82:745–774.

25. Klafki HW, et al. (1992) Complete amino acid sequence determinations demonstrate identity of the urinary Bence Jones protein (BJP-DIA) and the amyloid fibril protein (AL-DIA) in a case of AL-amyloidosis. *Biochemistry* 31(12):3265–3272.
26. Huang DB, Ainsworth CF, Stevens FJ, Schiffer M (1996) Three quaternary structures for a single protein. *Proc Natl Acad Sci USA* 93(14):7017–7021.
27. Fändrich M, Dobson CM (2002) The behaviour of polyamino acids reveals an inverse side chain effect in amyloid structure formation. *EMBO J* 21(21):5682–5690.
28. Lopez del Amo JM, et al. (2012) An asymmetric dimer as the basic subunit in Alzheimer's disease amyloid β fibrils. *Angew Chem Int Ed Engl* 51(25):6136–6139.
29. Schütz AK, et al. (2015) Atomic-resolution three-dimensional structure of amyloid β fibrils bearing the Osaka mutation. *Angew Chem Int Ed Engl* 54(1):331–335.
30. Teng PK, et al. (2012) Ribonuclease A suggests how proteins self-chaperone against amyloid fiber formation. *Protein Sci* 21(1):26–37.
31. Mishima T, et al. (2009) Residual structures in the acid-unfolded states of λ 6 proteins affect amyloid fibrillation. *J Mol Biol* 392(4):1033–1043.
32. Morris KL, et al. (2013) The structure of cross- β tapes and tubes formed by an octapeptide, α 5 β 1. *Angew Chem Int Ed Engl* 52(8):2279–2283.
33. Yolamanova M, et al. (2013) Peptide nanofibrils boost retroviral gene transfer and provide a rapid means for concentrating viruses. *Nat Nanotechnol* 8(2):130–136.
34. Reches M, Gazit E (2003) Casting metal nanowires within discrete self-assembled peptide nanotubes. *Science* 300(5619):625–627.
35. Holmes TC, et al. (2000) Extensive neurite outgrowth and active synapse formation on self-assembling peptide scaffolds. *Proc Natl Acad Sci USA* 97(12):6728–6733.
36. Ludtke SJ, Baldwin PR, Chiu W (1999) EMAN: Semiautomated software for high-resolution single-particle reconstructions. *J Struct Biol* 128(1):82–97.
37. Frank J, et al. (1996) SPIDER and WEB: Processing and visualization of images in 3D electron microscopy and related fields. *J Struct Biol* 116(1):190–199.
38. Grigorieff N (2012) *bfactor*, Version 1.04. Available at grigoriefflab.janelia.org/bfactor. Accessed May 2016.
39. Emsley P, Lohkamp B, Scott WG, Cowtan K (2010) Features and development of Coot. *Acta Crystallogr D Biol Crystallogr* 66(Pt 4):486–501.
40. Pettersen EF, et al. (2004) UCSF Chimera—A visualization system for exploratory research and analysis. *J Comput Chem* 25(13):1605–1612.
41. Maurer-Stroh S, et al. (2010) Exploring the sequence determinants of amyloid structure using position-specific scoring matrices. *Nat Methods* 7(3):237–242.
42. Fernandez-Escamilla AM, Rousseau F, Schymkowitz J, Serrano L (2004) Prediction of sequence-dependent and mutational effects on the aggregation of peptides and proteins. *Nat Biotechnol* 22(10):1302–1306.
43. Frousios KK, Iconomidou VA, Karletidi CM, Hamodrakas SJ (2009) Amyloidogenic determinants are usually not buried. *BMC Struct Biol* 9:44.
44. Garbuzynskiy SO, Lobanov MY, Galzitskaya OV (2010) FoldAmyloid: A method of prediction of amyloidogenic regions from protein sequence. *Bioinformatics* 26(3):326–332.
45. Conchillo-Solé O, et al. (2007) AGGRESCAN: A server for the prediction and evaluation of "hot spots" of aggregation in polypeptides. *BMC Bioinformatics* 8:65.
46. Puchtler H, Sweat F, Levine M (1962) On the binding of Congo Red amyloid. *J Histochem Cytochem* 10:355–364.
47. Wall JS, Simon MN (2001) Scanning transmission electron microscopy of DNA-protein complexes. *Methods Mol Biol* 148:589–601.
48. Diaz-Avalos R, King CY, Wall J, Simon M, Caspar DL (2005) Strain-specific morphologies of yeast prion amyloid fibrils. *Proc Natl Acad Sci USA* 102(29):10165–10170.
49. Tang G, et al. (2007) EMAN2: An extensible image processing suite for electron microscopy. *J Struct Biol* 157(1):38–46.
50. Schrödinger, LLC (2014) *The PyMOL Molecular Graphics System, Version 1.7.4* (Schrödinger, New York).
51. Vilar M, et al. (2008) The fold of alpha-synuclein fibrils. *Proc Natl Acad Sci USA* 105(25):8637–8642.
52. Creighton TE (1993) *Proteins—Structures and Molecular Properties* (Freeman, New York), 2nd Ed.